Correction of phase wrapping artifacts in grating-based hard x-ray tomography

Griffin Rodgers, Georg Schulz, Hans Deyhle, Shashidhara Marathe, Christos Bikis, et al.

SPIE.

Correction of phase wrapping artifacts in grating-based hard X-ray tomography

Griffin Rodgers[a], Georg Schulz[a], Hans Deyhle[a,b], Shashidhara Marathe[b], Christos Bikis[a], Bert Müller[a], and Timm Weitkamp[c]

[a]Biomaterials Science Center, University of Basel, 4123 Allschwil, Switzerland
[b]Diamond Light Source Ltd., Didcot OX11 0DE, UK
[c]Synchrotron Soleil, 91192 Gif-sur-Yvette, France

ABSTRACT

X-ray grating interferometry (XGI) is a phase-contrast imaging technique that allows for a quantitative measurement of the refractive index with high density resolution in a model-independent manner—i.e. without *a priori* knowledge of the specimen composition. However, the retrieval of the X-ray wavefront phase shift relies on the accurate measurement of the interference pattern phase shift, making XGI vulnerable to phase wrapping when the interference pattern phase shift, related to the derivative of the wavefront phase shift, is large. Standard procedure for avoiding phase wrapping involves submerging the specimen in a water bath to reduce the mismatch of the index of refraction at the boundaries, but this requires a top-down rotation stage and is susceptible to gas bubble formation inside the water bath. Our team has presented an algorithm to remove phase wrapping artifacts for cylindrically shaped specimens that is applied to the phase-retrieved sinogram. This algorithm models and replaces phase-wrapped data to prevent the spread of "cupping" artifacts due to the integration of the differential phase during reconstruction. We give a criterion for selecting the modeling parameters so that the resulting measurement of the index of refraction matches the results of measurements without phase wrapping. We also apply this technique to cases where phase wrapping occurs at multiple interfaces. This algorithm allows for XGI measurements without a water bath and top-down rotation stage at synchrotron and laboratory facilities, especially as sensitivity increases.

Keywords: X-ray phase tomography, X-ray grating interferometry, phase wrapping, artifact correction, algorithms

1. INTRODUCTION

1.1 X-ray grating interferometry

X-ray grating interferometry (XGI) is a model-independent phase-contrast method that provides access to the differential phase shift of the X-ray wavefront. This allows for the quantitative measurement of the decrement of the real part of the refractive index δ.[1] XGI is particularly useful for the three-dimensional visualization of biological soft tissues, which are composed of low-Z elements and therefore exhibit weak X-ray absorption.[2,3]

XGI is based on a beam-splitting grating that creates an interference pattern at fractional Talbot distances downstream.[4] This pattern can be directly read by the detector in so-called single grating mode[5] or, more commonly, a second analyzer grating with period matching the interference pattern is placed in front of the detector to read out the interference pattern of the beam-splitter grating.[1] A specimen placed in the beam path produces a phase shift, which in turn leads to a lateral shift in the interference pattern ϕ. This interference pattern phase shift is measured for each detector pixel and in the case of tomography for each projection angle.

The interference pattern shift ϕ is related the differential phase shift through

$$\phi(x,\theta) = \frac{2\pi d}{p_2} \times \frac{\partial}{\partial x}\left[\int \delta(x',y')dy\right], \tag{1}$$

where d is the propagation distance, p_2 the period of the analyzer grating, and the integral taken over the X-ray path through the specimen at rotation angle θ. The differential phase shift can be integrated before or during reconstruction, e.g. with a filtered backprojection with modified kernel.[6] This provides an isotropic representation of the δ values in three-dimensional space.

1.2 Phase wrapping

1.2.1 Conditions

The measured signal in XGI is the interference pattern phase shift ϕ, which is naturally restricted to the range $\phi \in (-\pi, \pi]$. From Eq. 1, this range will be exceeded at large propagation distances, small fringe period, and most notably at interfaces with large δ changes over a short distance. Specimen edges are therefore highly susceptible to so-called phase wrapping, especially as XGI setups become more sensitive.

Assuming certain idealized specimens, the extent of phase wrapping for a given XGI setup can be calculated by solving Eq. 1 for $|\phi(x_{pw})| = \pi$. Phase wrapping will occur between the specimen edge and

$$x_{pw} = R/\sqrt{1 + (4d\delta/p_2)^2} \tag{2}$$

for a uniform cylindrical specimen of radius R.[7]

1.2.2 Artifacts

Phase wrapping leads to a measured interference pattern phase shift ψ with smaller absolute value, $|\psi| < |\phi|$. Integration of the differential phase shift leads to reduced measured phase shift across the specimen and particularly at the edges. This leads to an overall reduction of the reconstructed δ values and an additional reduction at the edges, leading to the characteristic cupping artifacts.
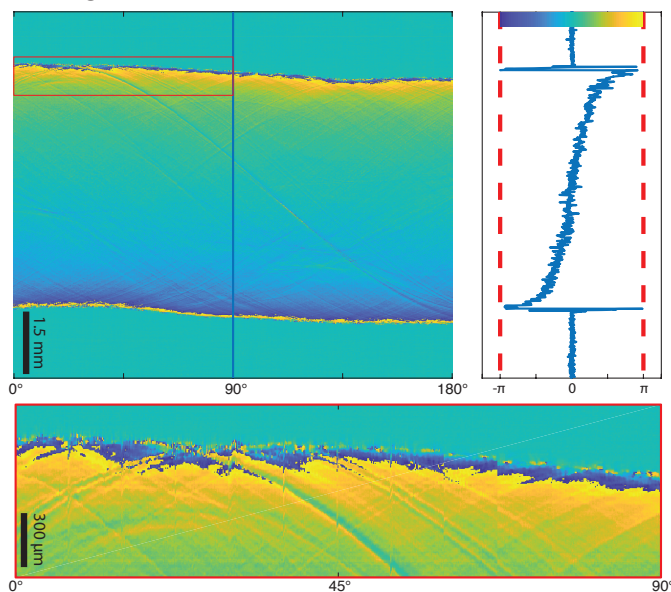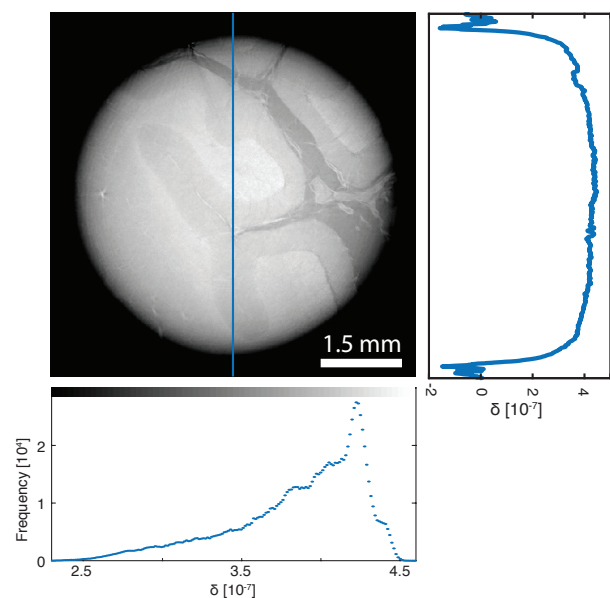
Figure 1. Phase wrapping and reconstruction artifacts. Phase wrapped sinogram (left) and resulting reconstruction (right) of a paraffin-embedded human cerebellum specimen. The reconstruction suffers from characteristic "cupping" artifacts seen in the line profile, which arise from the lower measured interference pattern phase shift in the wrapped regions and the integration step during reconstruction. The histogram shows that quantitative measurements of tissue density are impossible. Visualization is difficult because cupping is large compared to the δ variations between anatomical features.
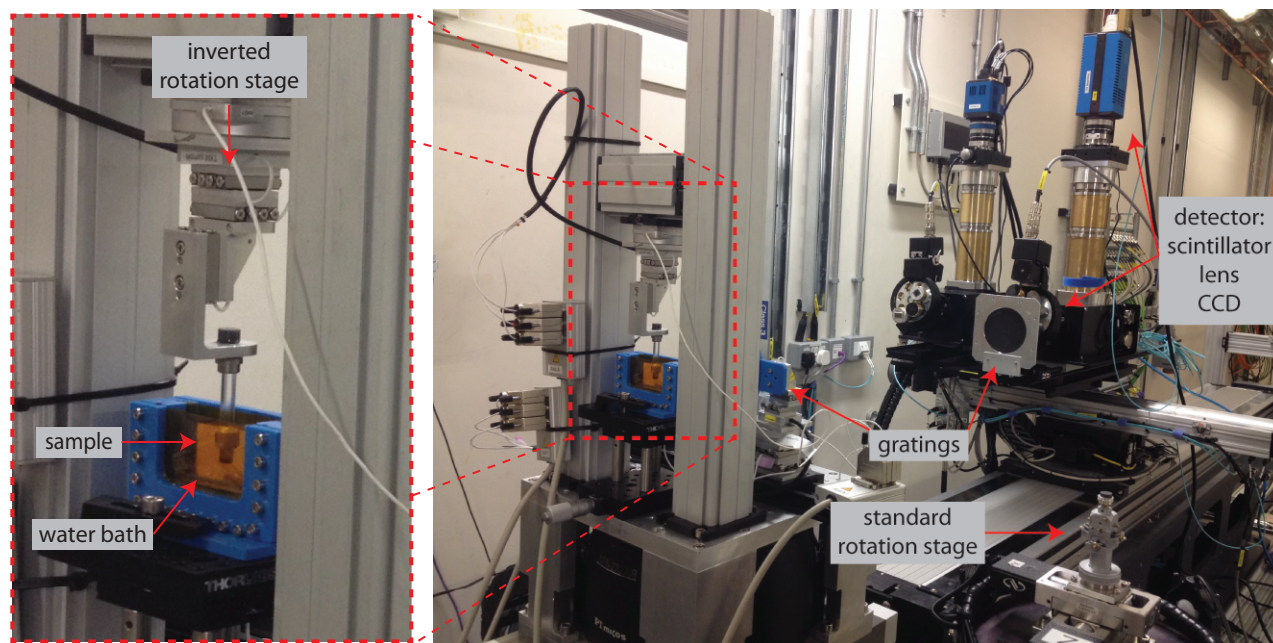
Figure 2. A grating interferometry setup including water bath to avoid phase wrapping. To submerge the specimen in the water, an inverted rotation stage is needed (zoom on left). This requires a dedicated setup. The standard rotation stage for tomography is unused on the right. Our correction alleviates the need for this dedicated setup with water bath and inverted rotation stage. This was the temporary setup on the Diamond Manchester Imaging Beamline (I13-2, Diamond Light Source, Didcot, UK).

Fig. 1 shows an example of a phase wrapped dataset obtained from a cylindrical piece of a paraffin-embedded human cerebellum. The sinogram shows a region of phase wrapping along the specimen-air interface. The edges with $|\psi| < |\phi|$ are seen in the line profile. The reconstructed slice and line profile demonstrate cupping artifacts and the edges of the specimen have negative δ values. The histogram shows that the δ values throughout the specimen are smeared out and no quantitative measurements of δ are possible. Even qualitative assessment can be difficult when the cupping is larger than the δ variations within the specimen.

1.2.3 Avoiding phase wrapping

In order to avoid phase wrapping at the specimen edges, the specimen is typically submerged in a liquid that matches the specimen δ. Fig. 2 shows the temporary setup for XGI at the Diamond Manchester Imaging Beamline (I13-2, Diamond Light Source, Didcot, UK),[8] which includes a water bath.

This method, however, has several drawbacks. The inverted rotation stage requires a dedicated setup that can be time-consuming to assemble and less stable than standard rotation stages. The width of the liquid bath should be well-matched to the specimen size to keep the loss of photons reasonable low. Finally, gas bubbles can also form at the specimen-liquid interface, causing severe motion artefacts. Therefore, a software correction is highly desirable.

Phase wrapping occurs in many measurement techniques several phase unwrapping approaches are commonly available. XGI requires dedicated methods for phase unwrapping because the ϕ changes may be greater than 2π over a short span. Moreover, the linear relationship between ϕ and the differential phase shift may not hold for strong wavefront curvature.

Previous studies have shown information from the attenuation channel and the assumed relationship between the attenuation and phase shift gradient can be used to identify and correct wrapped pixels.[9, 10] This approach works well for phase wrapping of only several pixels, however at specimen edges wrapping may extend over a large region (cf. Eq. 2) where the gradient of the attenuation signal is small. This can be seen from the sinograms
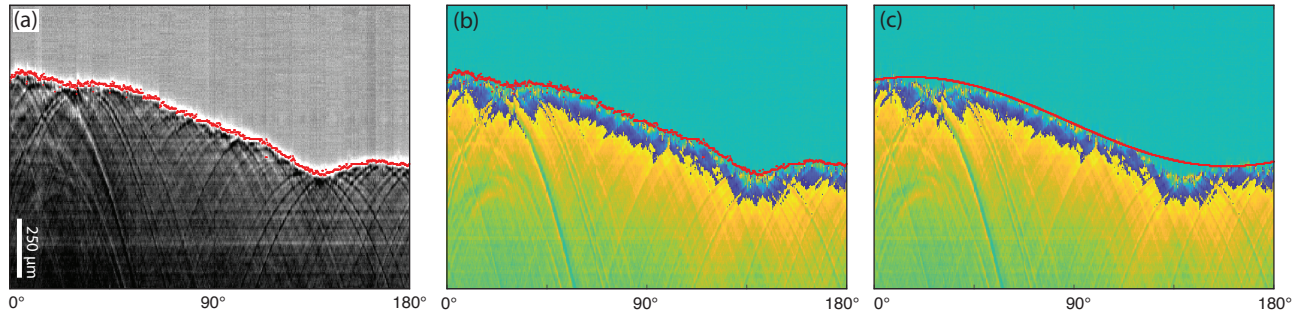
Figure 3. Identifying the specimen edges in the sinogram. (a) Specimen edges can be found from thresholding the absorption channel sinogram, which shows edge enhancement. (b) These edge positions are transferred to the differential phase sinogram. (c) The edges are smoothed, in this case a sinosoidal fit is applied therefore assuming a cylindrical specimen. (d) A replacement window is defined around the determined edge positions to ensure all wrapped data is replaced. A larger window is useful for applying the correction to many slices, though it sacrifices more of the specimen. Grayscale corresponds to (a) $t \in [0.8, 1.1]$ and (b-d) $\phi \in [-\pi, \pi]$.

in Fig. 3 (a) and (b), where the phase wrapping extends several tens of pixels inside of the edge regions where attenuation is rapidly changing.

Estimation of the phase and unwrapping through multiple energy measurements has also been suggested,[11] though not all XGI setups allow for multiple energies and more experimental time is needed.

An early version of the correction presented here was previously used in the study published in Ref. 12. The correction was then refined and presented in Ref. 13. Here, we describe the working principles in more detail, discuss the practical usage, and discuss extensions as well as challenges for this approach.

2. PROPOSED CORRECTION ALGORITHM

Rather than unwrapping individual pixels, our approach is to sacrifice the wrapped regions to avoid cupping and other artifacts that affect the non-wrapped regions during integration and reconstruction. Phase wrapped regions are replaced by ϕ_m calculated from a model specimen with shape and composition similar to the real specimen. Our algorithm consists of the following steps:

1. Find specimen edges

2. Model the specimen

3. Replace wrapped regions and reconstruct

4. Repeat 2 and 3 with different model δ until cupping is minimized

Each of these steps is discussed in more detail in the following sections.

2.1 Finding wrapped regions

The outer edges of the specimen should be determined in order to create a model specimen with the same shape as the real specimen. This involves a simple segmentation that can be accomplished with established methods in either the projection or sinogram.

Fig. 3 shows an example of edge determination for the case presented in Fig. 1. The absorption information is used because strong edge enhancement is present. The pixel with the maximum intensity value for each angle is selected and indicated in part (a). These selected pixels are transferred to the differential phase sinogram (b).

A sinosoidal fit is made to smooth the edge positions (c) with the benefit of simple interpretation as a cylindrical shaped model specimen. In general, some smoothing should be applied to account for noise that creates jagged specimen edges. For other specimen shapes, fitting an appropriate function or using dedicated smoothing techniques is preferable (more detail in the section below).
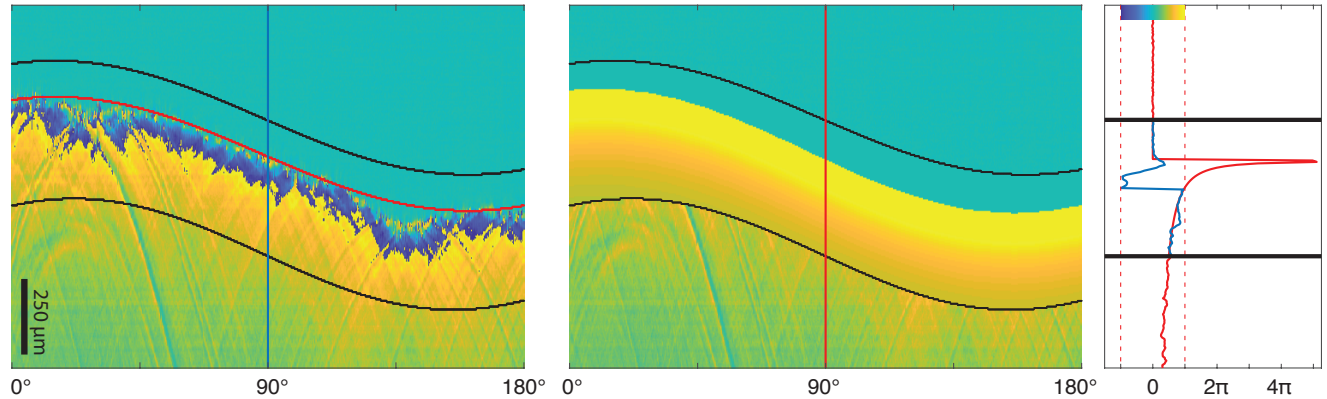
Figure 4. Replacing phase wrapped data. The phase wrapped sinogram (left) is replaced with modelled data (right) within a defined window. Line profiles indicate the model data extending beyond $(-\pi, \pi]$ where the previous data had been wrapped. The modelled data provides the missing differential phase information during the integration step of reconstruction, though it does not provide details in the regions that are replaced. Though not the case here, discontinuities between modelled and real data at the replacement window edge are tolerable to some extent.

2.2 Modelling the specimen

We always assume a uniform specimen with δ_m and calculate the projected thickness for each rotation angle $t(x, \theta)$. A discrete derivative replaces the derivative in Eq. 1 to create the modelled data ϕ_m given by

$$\phi_m(x, \theta) = \frac{2\pi d}{p_2} \times \delta_m \times \frac{\Delta}{\Delta x} t(x, \theta). \tag{3}$$

The case presented in Fig. 3 assumes a cylindrical specimen. Here, $t(x, \theta) = \sqrt{R^2 - (x - x_0(\theta))^2}$ with specimen center x_0 and radius R calculated from the edge positions found in Step 1.

When simply modelled shapes do not match the actual shape, low frequency artifacts appear in the reconstruction. A better approach, though more time consuming, is to segment the specimen edges in the absorption reconstruction or in the sinogram and convert from sinogram to reconstruction coordinates, fill the shape, and numerically calculate the Radon transform to produce $t(x, \theta)$. Then Eq. 3 provides the modelled sinogram to replace the phase wrapped data.

2.3 Replacing and reconstructing

A window around the edges found in Step 2 is defined for replacement with the modelled data. This window should be large enough to contain all of the phase wrapped data. A larger window is often preferable as a one-size-fits-all approach for correcting many slices, though it has the drawback of sacrificing more of the real data.

An example is seen in Fig. 4 (left), where the window is defined by a number of pixels above and below the edge positions. The modelled data is inserted in this window (center). Line profiles (right) show that ϕ_m matches the real data well at the edges of the replacement window.

A discontinuity at the replacement window will cause gradients in the reconstructed δ near the window edges. A small jump is tolerable, particularly when structures of interest are far from the replacement window. Large discontinuities may be due to incorrect δ_m or poorly selected edge pixels.

2.4 Determining the correct modelling parameters

Fig. 5 shows the procedure for the selection of the modelling parameters. Typically, the edge positions and replacement window are fixed, then the only parameter to tune is δ_m. A small (large) δ_m leads to downwards (upwards) cupping, as seen in Fig. 5 (a). The ideal δ_m should minimize the cupping, therefore homogenous
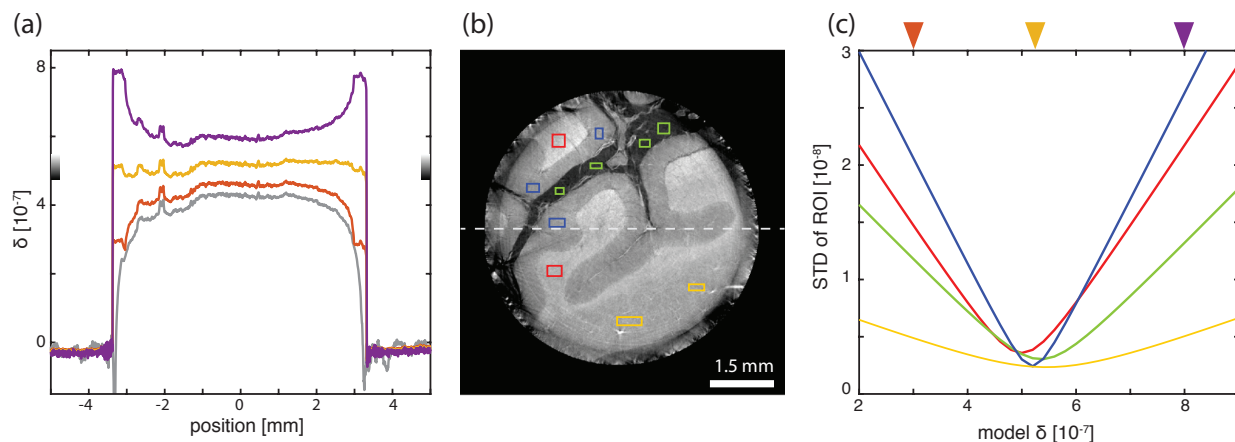
Figure 5. Selecting the model δ value. (a) Line profiles through the reconstruction with uncorrected sinogram (gray) and sinograms corrected with model $\delta = 2 \times 10^{-7}$ (orange), $\delta = 5.25 \times 10^{-7}$ (yellow), and $\delta = 8 \times 10^{-7}$ (purple). Too small (large) δ results in downward (upward) cupping. (b) Regions of interest (ROIs) within homogenous areas of the specimen are determined in the reconstruction. The sacrificed region where real data has been replaced is visible around the specimen edges. (c) The standard deviation of the ROIs is measured as a function of the model δ. The optimal model δ is that which minimizes the standard deviation of these ROIs. The line profiles in (a) correspond to model δ indicated by the triangles.

regions of interest (ROIs) are selected in the specimen, see Fig. 5 (b), and the standard deviation is measured over a range of δ_m, Fig. 5 (c). The best choice of δ_m minimizes the standard deviation. In the case of Fig. 5, the average of the value minimizing each ROI is selected for δ_m.

If there is no minimum or if the best δ_m varies greatly for each ROI, it is likely a poor model specimen shape and/or replacement window has been selected. ROI selection should also cover various regions of the specimen to ensure cupping is fully considered.

3. RESULTS AND DISCUSSION

3.1 Experimental validation

The performance of the proposed algorithm was evaluated in two experiments.[13] In both cases, a specimen was measured in a water bath as a reference without phase wrapping. The water was then removed to produce a wrapped dataset. The correction was applied and compared with the dataset without wrapping.

The first specimen was a stack of plastic phantoms consisting of polypropylene (PP), two types of polyvinyl chloride (PVC 1 and PVC 2), and polyoxymethylene (POM). Since the surrounding medium was different, the $\Delta\delta$ from PP was measured for each dataset. The results are presented in Table 1. The not wrapped dataset shows good agreement with the corrected dataset. The larger standard deviation for the corrected datasets is due to a combination of different photon statistics and cupping that is not fully removed.

Table 1. Relative δ mean and standard deviation measured in plastic phantoms without phase wrapping, with phase wrapping, and with phase wrapping and correction. Phantoms consisted of polypropylene (PP), two types of polyvinyl chloride (PVC 1 and PVC 2), and polyoxymethylene (POM). All values are $\times 10^{-8}$ and mean values are relative to PP.

	PP		PVC 1		PVC 2		POM	
	$\Delta\delta$	σ_δ	$\Delta\delta$	σ_δ	$\Delta\delta$	σ_δ	$\Delta\delta$	σ_δ
not wrapped	0.00	0.47	15.40	0.37	18.73	0.26	22.03	0.31
wrapped	0.00	3.10	9.15	0.37	10.16	2.84	11.42	1.99
corrected	0.00	0.62	15.12	0.37	19.38	0.81	23.15	0.39
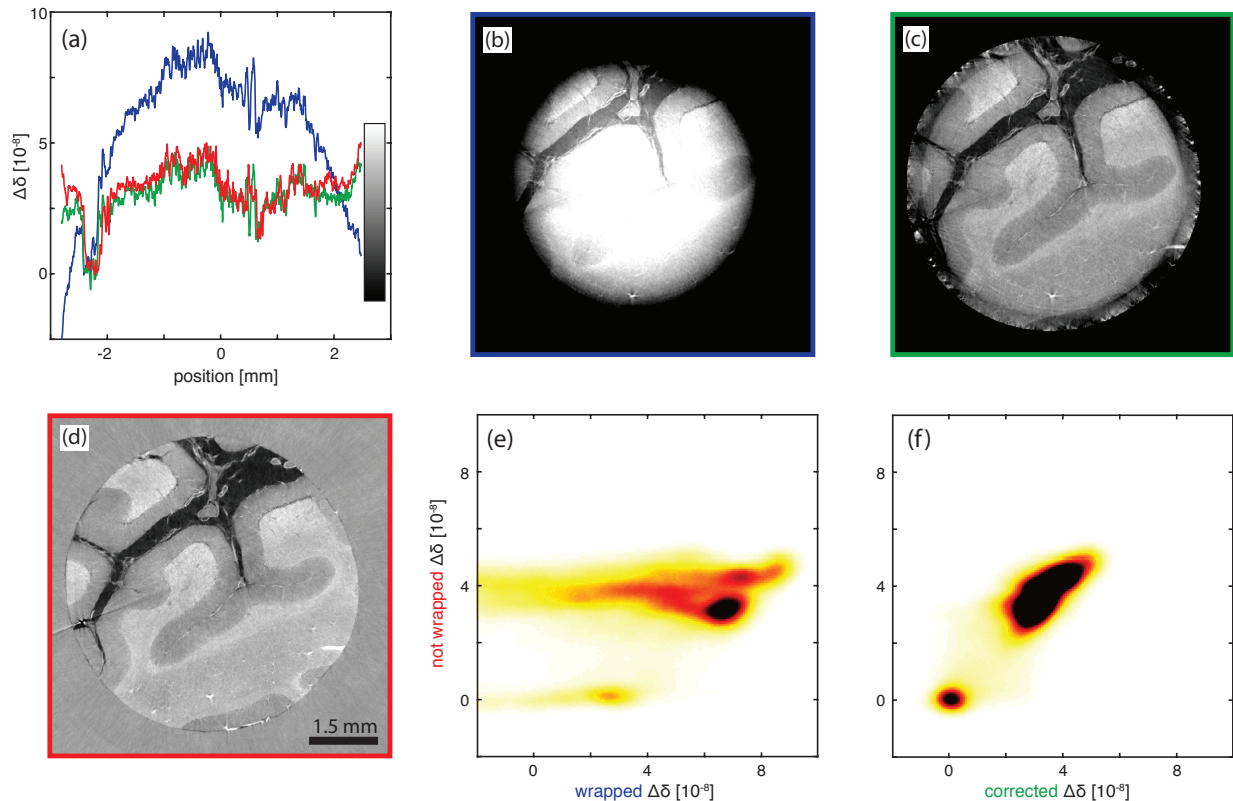
Figure 6. Phase wrapping correction for paraffin-embedded cerebellum specimen. (a) line profiles through the reconstructed slices of the (b) wrapped, (c) wrapped and corrected, and not wrapped (d) datasets. The surrounding medium was air (b & c) and water (d). Bivariate histograms of (b) and (d) show the cupping artifacts introduced by phase wrapping. The agreement between the corrected dataset and the not wrapped dataset are clear from their bivariate histogram (e) and line profiles (a). Both histograms contained 200×200 bins and were scaled with Frequency $\in [0, 10^4]$ and a circular mask excluded specimen edges and surrounding medium.

The performance of the correction algorithm for a cylindrical punch of paraffin-embedded human cerebellum is summarized in Fig. 6. Line profiles (a) and visual comparison of representative reconstructed slices (b-d) show strong agreement between the corrected and not wrapped datasets inside the replacement window. The quantitative accuracy is demonstrated by bivariate histograms of the wrapped (e) and corrected datasets (f) with the not wrapped dataset. The bivariate histogram in (f) lies mostly on the diagonal, indicating a strong agreement between the measured $\Delta\delta$ of the datasets.

3.2 Extensions and challenges

As discussed in Section 2.2, this algorithm supports the correction of more than just cylindrically shaped specimens. It can be successfully applied to cases with multiple phase wrapped interfaces. This finding is shown in Fig. 7 (a & b), where wrapping occurred at the Eppendorf-air and the paraffin-Eppendorf interfaces (the latter likely due to trapped air bubbles). The outer edges were non-cylindrical due to heat-induced deformation of the Eppendorf container, therefore a smoothing filter was applied rather than a sinoisodal fit.

A more challenging case is presented in Fig. 7 (c & d), which is a dried mouse brain specimen in an Eppendorf tube. The Eppendorf walls and the brain's outer edge show phase wrapping that can be handled by the approach presented here. However, air-tissue interfaces within the dried brain create many small phase wrapping regions. Modelling this specimen's interior would be complex and sacrifice too much of the specimen area. In this case, a complementary method based on attenuation data may be better suited for the interior wrapping.[9,10] Specimens such as this one can not be embedded in a liquid bath, as water would re-hydrate the specimen and other liquids may not fill the specimen interior.
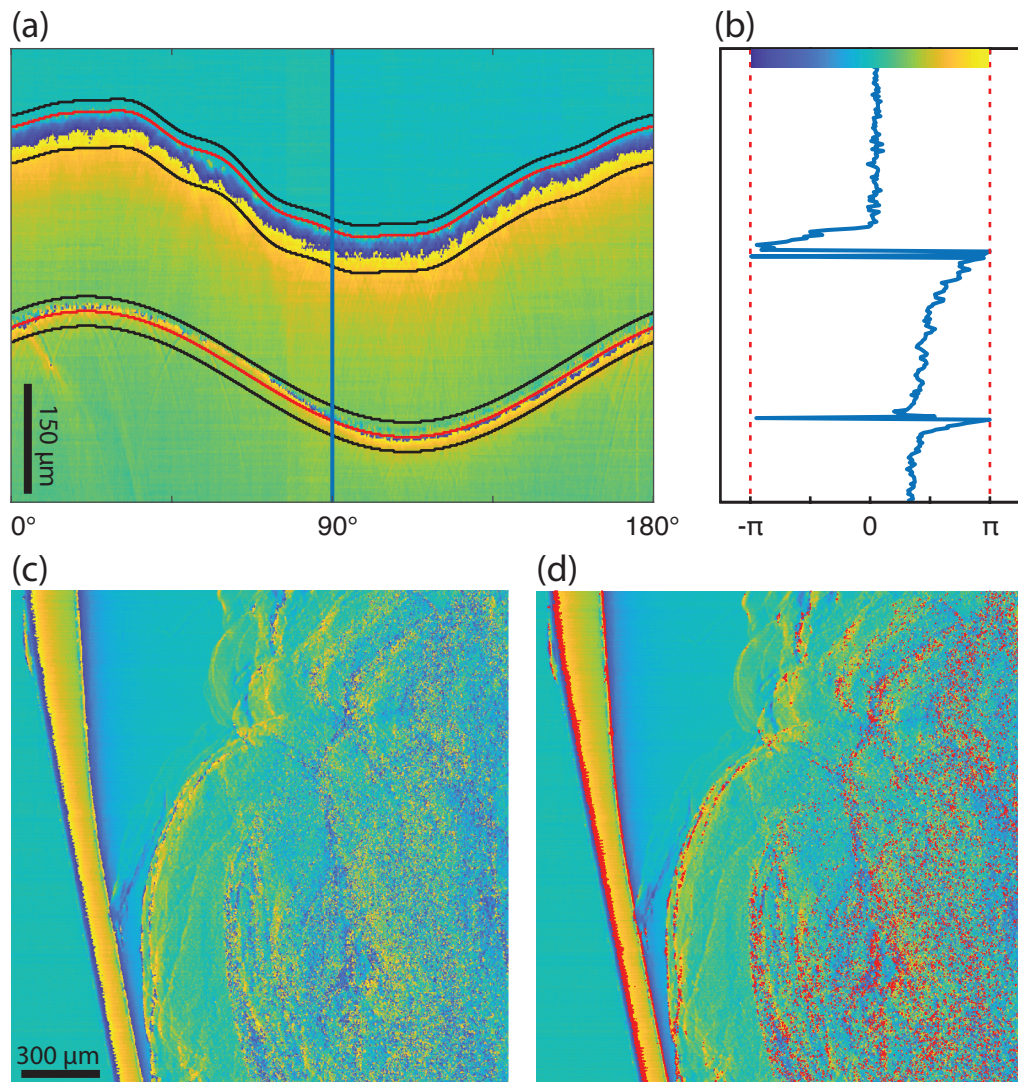
Figure 7. Challenges and extensions for this correction algorithm. (a & b) A sinogram that has multiple phase wrapped interfaces (specimen: paraffin wax in an Eppendorf container). The proposed method can be applied for each interface. The outer edge is not cylindrical and is therefore modelled by determining specimen outline from the detected edge and numerical calculation of the Radon transform. (c & d) A specimen with many interior phase-wrapped interfaces presents major challenges (specimen: dried mouse brain in an Eppendorf container). Pixels likely suffering from phase wrapping are marked in (d) (threshold with $\phi > 2.75$ radians). The container walls and specimen edge can be corrected with the proposed method. Interior wrapping is better suited with a complementary method, e.g. Ref. 10 or Ref. 9.

4. CONCLUSION

The proposed algorithm allows for correcting phase wrapping artifacts and the recovery of accurate $\Delta\delta$ values within the phase wrapped edges of the specimen. The proposed method has been demonstrated for the case of cylindrical specimens, but the basis of the correction can be extended to more complex specimen geometries as outlined above. We envision that the proposed correction can be combined with other approaches to treat more complex cases where wrapping is not only at the outer specimen boundaries. The proposed correction algorithm should alleviate the need for measuring with the specimen in a water or oil bath, therefore simplifying the experimental setup for the rather time-consuming XGI combined with tomographic imaging.

ACKNOWLEDGMENTS

REFERENCES

[1] Weitkamp, T., Diaz, A., David, C., Pfeiffer, F., Stampanoni, M., Cloetens, P., and Ziegler, E., "X-ray phase imaging with a grating interferometer," *Opt. Express* **13**(16), 6296–6304 (2005).

[2] Momose, A., "Recent advances in x-ray phase imaging," *Jpn. J. Appl. Phys.* **44**(9R), 6355 (2005).

[3] Schulz, G., Weitkamp, T., Zanette, I., Pfeiffer, F., Beckmann, F., David, C., Rutishauser, S., Reznikova, E., and Müller, B., "High-resolution tomographic imaging of a human cerebellum: comparison of absorption and grating-based phase contrast," *J. Royal Soc. Interface* **7**(53), 1665–1676 (2010).

[4] Momose, A., Kawamoto, S., Koyama, I., Hamaishi, Y., Takai, K., and Suzuki, Y., "Demonstration of x-ray talbot interferometry," *Jpn. J. Appl. Phys.* **42**(7B), L866 (2003).

[5] Thalmann, P., Bikis, C., Hipp, A., Müller, B., Hieber, S., and Schulz, G., "Single and double grating-based x-ray microtomography using synchrotron radiation," *Appl. Phys. Lett.* **110**(6), 061103 (2017).

[6] Pfeiffer, F., Bunk, O., Kottler, C., and David, C., "Tomographic reconstruction of three-dimensional objects from hard x-ray differential phase contrast projection images," *Nucl. Instrum. Methods A* **580**(2), 925–928 (2007).

[7] Li, K., Zambelli, J., Bevins, N., Ge, Y., and Chen, G.-H., "Spatial resolution characterization of differential phase contrast ct systems via modulation transfer function (mtf) measurements," *Phys. Med. Biol.* **58**(12), 4119 (2013).

[8] Rau, C., "Imaging with coherent synchrotron radiation: X-ray imaging and coherence beamline (i13) at diamond light source," *Synchrotron Radiat. News* **30**(5), 19–25 (2017).

[9] Haas, W., Bech, M., Bartl, P., Bayer, F., Ritter, A., Weber, T., Pelzer, G., Willner, M., Achterhold, K., Durst, J., Michel, T., Prümmer, M., Pfeiffer, F., Anton, G., and Hornegger, J., "Phase-unwrapping of differential phase-contrast data using attenuation information," in [*Medical Imaging 2011: Image Processing*], **7962**, 79624R, International Society for Optics and Photonics (2011).

[10] Jerjen, I., Revol, V., Schuetz, P., Kottler, C., Kaufmann, R., Luethi, T., Jefimovs, K., Urban, C., and Sennhauser, U., "Reduction of phase artifacts in differential phase contrast computed tomography," *Opt. Express* **19**(14), 13604–13611 (2011).

[11] Epple, F., Potdevin, G., Thibault, P., Ehn, S., Herzen, J., Hipp, A., Beckmann, F., and Pfeiffer, F., "Unwrapping differential x-ray phase-contrast images through phase estimation from multiple energy data," *Opt. Express* **21**(24), 29101–29108 (2013).

[12] Zanette, I., Weitkamp, T., Lang, S., Langer, M., Mohr, J., David, C., and Baruchel, J., "Quantitative phase and absorption tomography with an x-ray grating interferometer and synchrotron radiation," *Phys. Status Solidi A* **208**(11), 2526–2532 (2011).

[13] Rodgers, G., Schulz, G., Deyhle, H., Marathe, S., Bikis, C., Weitkamp, T., and Müller, B., "A quantitative correction for phase wrapping artifacts in hard x-ray grating interferometry," *Appl. Phys. Lett.* **113**(9), 093702 (2018).